

**Fig. 4.** Real-time detection of  $\text{Ca}^{2+}$  ions. **(A)** Plot of conductance versus time for a calmodulin-terminated SiNW, where region 1 corresponds to buffer solution, region 2 corresponds to the addition of  $25 \mu\text{M}$   $\text{Ca}^{2+}$  solution, and region 3 corresponds to pure buffer solution. **(B)** Conductance versus time for an unmodified SiNW; regions 1 and 2 are the same as in **(A)**. Arrows mark the points when solutions were changed. Calmodulin-modified NWs were prepared by placing a drop ( $\sim 20 \mu\text{l}$ ) of calmodulin solution ( $250 \mu\text{g/ml}$ ) on SiNW for 1 hour and then rinsing with water for three times.

when a  $\text{Ca}^{2+}$ -free buffer was subsequently flowed through the device. Control experiments carried out with unmodified SiNWs (Fig. 4B) did not exhibit a conductance change when  $\text{Ca}^{2+}$  is added and thus demonstrate that the calmodulin receptor is essential for detection. In addition, the observed conductance decrease in modified SiNWs is consistent with expected chemical gating by positive  $\text{Ca}^{2+}$ , and the estimated dissociation constant,  $10^{-5}$  to  $10^{-6}$  M, is consistent with the reported  $K_d$  for calmodulin (27).

**References and Notes**

1. P. Bergveld, *IEEE Trans. Biomed. Eng.* **BME-19**, 342 (1972).
2. G. F. Blackburn, in *Biosensors: Fundamentals and Applications*, A. P. F. Turner, I. Karube, G. S. Wilson, Eds. (Oxford Univ. Press, Oxford, 1987), pp. 481–530.
3. D. G. Hafeman, J. W. Parce, H. M. McConnell, *Science* **240**, 1182 (1988).
4. F. Seker, K. Meecker, T. F. Kuech, A. B. Ellis, *Chem. Rev.* **100**, 2505 (2000).
5. S. J. Tans, A. R. M. Verschueren, C. Dekker, *Nature* **393**, 49 (1999).
6. P. G. Collins, M. S. Arnold, P. Avouris, *Science* **292**, 706 (2001).
7. Y. Cui, X. Duan, J. Hu, C. M. Lieber, *J. Phys. Chem. B* **104**, 5213 (2000).
8. Y. Cui, C. M. Lieber, *Science* **291**, 851 (2001).
9. X. Duan, Y. Huang, Y. Cui, J. Wang, C. M. Lieber, *Nature* **409**, 66 (2001).
10. Y. Huang, X. Duan, Q. Wei, C. M. Lieber, *Science* **291**, 891 (2001).
11. J. Kong et al., *Science* **287**, 622 (2000).
12. R. K. Iler, *The Chemistry of Silica* (Wiley, New York, 1979).

13. P. N. Bartlett, in *Handbook of Chemical and Biological Sensors*, R. F. Taylor, J. S. Schultz, Eds. (IOP Publishing, Philadelphia, 1996), pp. 139–170.
14. Y. Cui, L. J. Lauhon, M. S. Gudixsen, J. Wang, C. M. Lieber, *Appl. Phys. Lett.* **78**, 2214 (2001).
15. SiNWs with diameters of either 10 or 20 nm were suspended in ethanol and flow aligned on oxidized Si substrates ( $1$  to  $10 \text{ ohm-cm}$ , 600-nm oxide; Silicon Sense), and contact leads (50 nm Al or Ti + 100 nm Au) were defined with electron-beam lithography. The separation between contacts was typically 2 to 4  $\mu\text{m}$ . The conductance of SiNW devices as a function of time was determined directly with a computerized apparatus with lock-in amplifier (Stanford Research, SR 830); a 31-Hz sine wave with 30-mV amplitude at zero dc bias was used in most measurements. The conductances of the SiNW devices were between 500 and 2000 nS (resistance, 2 megohms to 500 kilohms). This relatively small range testifies to the good control of doping in our NWs.
16. Surface-functionalized SiNW devices were prepared by cleaning in an oxygen plasma (0.35 torr, 25 W power for 20 s) to remove contaminants, immersion in 1% ethanol solution of APTES (Aldrich) for 20 min, rinsing with ethanol for three times, followed by heating at  $120^\circ\text{C}$  for 5 min. The different pH solutions were made from 10 mM phosphate buffers with 100 mM NaCl. Solutions were flowed through PDMS microchannels (10, 17) (100- to 200- $\mu\text{m}$  width and height) at a flow rate of 0.5 ml/hour. The parasitic conductance through the solution was a constant (about 10 nS) and less than the signal from the SiNW (about 100 nS).
17. D. C. Duffy, J. C. McDonald, O. J. A. Schueller, G. M. Whitesides, *Anal. Chem.* **70**, 4974 (1998).
18. D. V. Vezenov, A. Noy, L. F. Rozsnyai, C. M. Lieber, *J. Am. Chem. Soc.* **119**, 2006 (1997).
19. G. H. Bolt, *J. Phys. Chem.* **61**, 1166 (1957).
20. Biotin-modified SiNWs were prepared by depositing a drop ( $\sim 20 \mu\text{l}$ ) of phosphate-buffered solution (PBS) ( $250 \mu\text{g/ml}$ ; pH 5.6) solution of biotinamidocaproyl-labeled bovine serum albumin (Sigma) on SiNWs for 2 hours, followed by a five times rinse with buffer

solution. The solutions used to probe biotin-streptavidin binding were 1 mM phosphate buffer (pH 9) with 10 mM NaCl. The d-biotin-saturated streptavidin solution was prepared by adding four equivalents of d-biotin (Sigma) to one equivalent of streptavidin. All the solutions used in biotin and m-antibiotin (Sigma) binding studies were 1 mM phosphate buffer (pH 7) with 5 mM NaCl. The parasitic conductance in these experiments,  $\leq 5$  nS, was substantially less than the sensor signal, 40 to 100 nS.

21. M. Wilchek, E. A. Bayer, *Methods Enzymol.* **184**, 49 (1990).
22. In addition, the detection sensitivity can be changed by the doping concentration and should enable single-molecule detection at sufficiently low concentration. As an example, a single charge on the NW surface will be detected if it generates a sufficiently large local potential barrier ( $>100$  meV at room temperature) for electronic motion. Assuming that a single charge is  $\sim 1$  nm away from a 20-nm-diameter NW, the carrier concentration will most likely be lower than the order of  $\sim 1000$  electrons/ $\mu\text{m}$  (or a few electrons/nm) for detection, which translates into  $3 \times 10^{18}$  to  $10^{19} \text{ cm}^{-3}$ .
23. L. Movileanu, S. Howorka, O. Braha, H. Bayley, *Nature Biotechnol.* **18**, 109 (2000).
24. R. C. Blake II, A. R. Pavlov, D. A. Blake, *Anal. Biochem.* **272**, 123 (1999).
25. H. Bagci, F. Kohen, U. Kuscuoğlu, E. A. Bayer, M. Wilchek, *FEBS Lett.* **322**, 47 (1993).
26. Sequence analysis shows that the binding region of antibiotin (IgG1) is positively charged at pH 7 (24). The remaining domains of this large protein are relatively distant from the SiNW and thus should have little effect on SiNW conductance.
27. C. B. Klee, T. C. Vanaman, *Adv. Protein Chem.* **35**, 213 (1982).
28. We thank L. Lauhon, L. Chen, and Q. Cui for helpful discussion and T. Deng for technical assistance. C.M.L. acknowledges support of this work by the Office of Naval Research and the Defense Advanced Projects Research Agency.

21 May 2001; accepted 23 July 2001

## Stable Ordering in Langmuir-Blodgett Films

Dawn Y. Takamoto,<sup>1</sup> Eray Aydil,<sup>1</sup> Joseph A. Zasadzinski,<sup>1\*</sup> Ani T. Ivanova,<sup>2</sup> Daniel K. Schwartz,<sup>2†</sup> Tinglu Yang,<sup>3</sup> Paul S. Cremer<sup>3</sup>

Defects in the layering of Langmuir-Blodgett (LB) films can be eliminated by depositing from the appropriate monolayer phase at the air-water interface. LB films deposited from the hexagonal phase of cadmium arachidate ( $\text{CdA}_2$ ) at pH 7 spontaneously transform into the bulk soap structure, a centrosymmetric bilayer with an orthorhombic herringbone packing. A large wavelength folding mechanism accelerates the conversion between the two structures, leading to a disruption of the desired layering. At pH  $> 8.5$ , though it is more difficult to draw LB films, almost perfect layering is obtained due to the inability to convert from the as-deposited structure to the equilibrium one.

Langmuir-Blodgett films are made by pulling a substrate through a monolayer of amphiphilic molecules at the air-water interface. Under the appropriate conditions, the monolayer is transferred to the substrate (1, 2). Although the LB technique has been used for decades, applications of the method have been frustrated by defects ranging from pinholes to larger scale reorganization of the layers (Fig. 1A) (3, 4). We show here that this reorgani-

zation is the progression from the as-deposited structure to the thermodynamic equilibrium structure. However, as Fig. 1B shows, the reorganization can be slowed to the point that nearly perfect LB multilayer films can be made by depositing from a different monolayer phase that exists at the air-water interface at pH  $> 8.5$ . The high-pH monolayer phase has a more condensed and lower energy lattice structure than the monolayer at pH

## REPORTS

7 (5–7). In addition to decreasing the driving force for reorganization, the better ordering at high pH greatly increases the viscosity of the monolayer, which, in addition to slowing the transformation to the equilibrium structure, complicates the deposition process.

Synchrotron x-ray diffraction and atomic force microscopy (AFM) have revealed a remarkably rich polymorphism for fatty acids and other amphiphilic molecules at the air-water interface (5) and in LB films (2, 8). On a subphase containing millimolar cadmium at pH 7, arachidic acid [ $\text{CH}_3(\text{CH}_2)_{18}\text{COOH}$ ] monolayers have short-ranged hexagonal order. LB monolayers deposited from these conditions are made of the fatty acid salt, two monovalent anionic fatty acids complexed with a single divalent cationic cadmium, as expected by charge neutralization (9, 10). Monolayer LB films deposited from pH 7 have a short-range hexagonal packing similar to that found at the air-water interface (Fig. 2A) (11, 12). However, LB films with three or more layers condense into an orthorhombic, herringbone packing with long-range, crystalline order (11, 13) (Fig. 2A). The reduction in area per molecule that accompanies this transition to the orthorhombic packing likely leads to the proliferation of pinholes in the deposited films. Corkery pointed out that the lattice parameters and symmetry measured for fatty acid salt LB multilayers were identical with the equilibrium structure of the corresponding bulk metal soaps (14). Hence, even three-layer LB films have evolved to the equilibrium structure under these conditions.

For cadmium and other fatty acid salts, the equilibrium structure is a centrosymmetric bilayer, with one fatty acid molecule on either side of a central metal ion (14). Before deposition, however, the air-water interface constrains the fatty acid salt to be asymmetric—the cadmium ion in the aqueous phase, with both alkane chains on the air side of the interface. The lack of long-range order and the larger area per molecule in the asymmetric monolayer reinforce the idea that the centrosymmetric packing is energetically favored; the asymmetric structure is likely strained and the alkane chains cannot pack efficiently (6, 7). A LB monolayer on a hydrophilic substrate, however, must retain the asymmetry of the air-water interface, which explains the differences observed between

LB monolayers and multilayers (15). The transition between these two configurations—the asymmetric structure enforced by LB deposition and the centrosymmetric structure favored by equilibrium—is the driving force behind LB film reorganization. As soon as three asymmetric monolayers have been deposited on the substrate, a headgroup-to-headgroup interface is formed that facilitates the exchange of ions between fatty acids as illustrated schematically in Fig. 2B. Equally important to the kinetics of the reorganization, the hexagonal packing at the air-water interface can condense into the bulk soap structure by shrinking in the next-nearest-neighbor (NNN) direction with only a negligible expansion in the nearest-neighbor (NN) direction (Fig. 2A). The cylindrical symmetry of the alkane chains in the hexagonal phase is broken on this transformation; there is a regular orientational ordering of the chains in the herringbone packing.

The conversion from the hexagonal struc-

ture present at the air-water interface at pH 7 to the equilibrium structure also leads to the large-scale disruption of the layering (Fig. 1A). To show the consequences of the reorganization, we deposited alternating layer LB films of cadmium stearate ( $\text{CdSt}_2$ ,  $\text{C}_{18}$  carbon chain) and cadmium lignocerate [ $\text{CdL}_2$ ,  $\text{C}_{24}$  carbon chain, deposited at  $32^\circ\text{C}$  (16)] at pH 7. The difference in layer thickness between these two fatty acids is easily resolved in AFM images. These films formed multilayer islands and holes with the equilibrium lattice structure (15), as did  $\text{CdA}_2$  (Fig. 1A). The roughness of the terraces did not increase during the reorganization, showing that the fatty acids from different layers did not mix at the molecular level. The area of the holes was roughly equal to the area of the multilayer islands, so there was negligible loss of material by solubilization (15).

During every “downstroke” in which the LB films are in the subphase, two asymmetric monolayers are present tail-to-tail (Fig. 3).

**Fig. 1.** AFM images (5  $\mu\text{m}$  by 5  $\mu\text{m}$ ) of 21-layer  $\text{CdA}_2$  films on silicon. The grayscale variations correspond to differences in film heights. (A) Film deposited at pH 7. (B) Film deposited at pH 8.8. Arachidic acid [ $\text{CH}_3(\text{CH}_2)_{18}\text{COOH}$ ] was spread from chloroform (Aldrich Chemical, highest available purity; Milwaukee, WI) at a concentration of 2 mg/ml onto an aqueous subphase (Milli-Q plus system, resistivity of 18.2 megohm; Bedford, MA) with 0.6 mM  $\text{CdCl}_2$  adjusted to pH 6.5 to 7 (A) using  $\text{NaHCO}_3$  or to pH 8.8 (B) using either ammonium hydroxide ( $\text{NH}_4\text{OH}$ ) or sodium hydroxide ( $\text{NaOH}$ ) (Aldrich Chemical, highest available purity) in a circular NIMA (Coventry, UK) trough. Depositions were done at room temperature and a surface pressure of 30.0 mN/m. Transfer speed was 2 mm/min, with transfer ratios about one. Freshly cleaved silicon wafers (Semiconductor Processing, Boston, MA) cleaned in a hot  $\text{H}_2\text{O}_2/\text{H}_2\text{SO}_4$  solution (3:7 ratio) were used as substrates. Imaging was done in air, using a Nanoscope III AFM (Digital Instruments, Santa Barbara, CA) at ambient temperature. A 10- $\mu\text{m}$  scanner with a silicon nitride tip with spring constant 0.6 N/m was used for imaging.

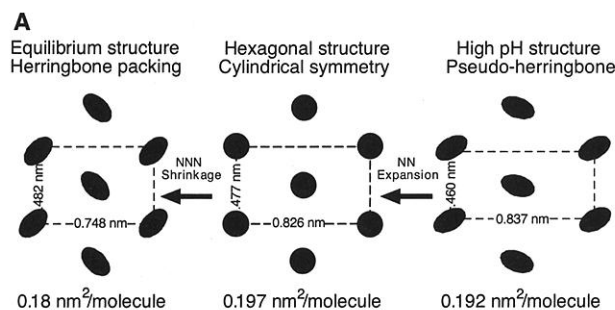
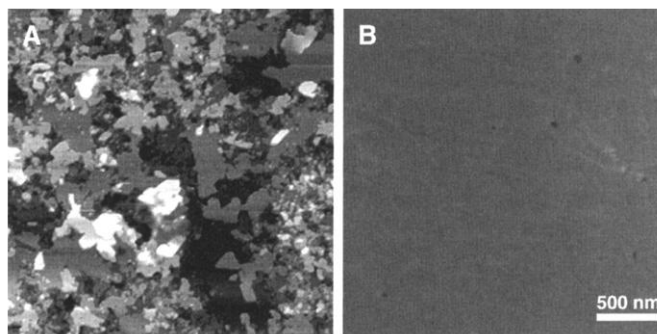


**Fig. 2.** (A) The three lattice structures of cadmium arachidate. The hexagonal structure is that present at the air-water interface at pH 7 and in monolayers deposited from pH 7. The equilibrium structure is present in three-dimensional crystals of cadmium arachidate and in multilayer Langmuir-Blodgett films deposited from pH 7 subphases. The high pH structure is present at the air-

water interface at pH >8.5 and has a different orientational ordering of the alkane chains. For this structure to transform into the equilibrium structure, the lattice must expand in the NN direction and go through the hexagonal packing. (B) Whenever a headgroup-headgroup (shaded circles) interface is formed during deposition, the cadmium ions and fatty acid molecules (straight lines) in the as-deposited, asymmetric configuration (left) can undergo a local exchange, forming the centrosymmetric configuration (right).

<sup>1</sup>Department of Chemical Engineering and Materials, University of California, Santa Barbara, CA 93106, USA. <sup>2</sup>Department of Chemistry, Tulane University, New Orleans, LA 70118, USA. <sup>3</sup>Department of Chemistry, Texas A&M University, College Station, TX 77843, USA.

\*To whom correspondence should be addressed. E-mail: gorilla@engineering.ucsb.edu

†Present address: Department of Chemical Engineering, University of Colorado, Boulder, CO 80309, USA.

One way to proceed to the equilibrium structure is via a large-scale bilayer folding process that leads to a headgroup-headgroup interface. Two possible mechanisms are shown in Fig. 3, "overturning" and "creeping." In the overturning mechanism, the bilayer folds back on itself and the bottom monolayer is now on top; the bilayer orientation is lost (15, 17). In the creeping mechanism, the bilayer detaches and slides over the remaining bilayer; the orientation of the bilayer is preserved. In both mechanisms, a new headgroup-headgroup interface is formed. This allows the transition between asymmetric and centrosymmetric structures, and a condensation of the hexagonal lattice into the lower energy equilibrium structure.

Figure 3 shows the two possible outcomes of these mechanisms on a reorganized film consisting of alternate layers of CdSt<sub>2</sub> and CdL<sub>2</sub>. Table 1 shows the predicted bilayer step heights for the two mechanisms, along with the average value of the step heights measured on LB films with CdSt<sub>2</sub> deposited first, followed by CdL<sub>2</sub>; or CdL<sub>2</sub> deposited first, followed by CdSt<sub>2</sub>. The measured step heights show that reorganization proceeds by the overturning mechanism. Overturning reorients the deposited layers, which is consistent with x-ray diffraction measurements of alternating layer films that show a partial intermixing of the layers (17, 18).

However, Fig. 1B shows that this reorganization does not occur if the LB films were deposited from a subphase of pH ≥ 8.5. Whereas the film deposited at pH 7 (Fig. 1A) had an overall height variation in excess of 12 nm (about two bilayers), the pH 8.8 film was flat to <1 nm (Fig. 1B). X-ray photoelectron spectroscopy (XPS) of the low-pH and high-pH films showed that the stoichiometry was about 40:1 of carbon to cadmium, confirm-

ing that the stoichiometry of both films was CdA<sub>2</sub> (9).

One reason that reorganization is inhibited in monolayers deposited from the higher pH is that the molecules are better ordered. X-ray diffraction by Leveiller *et al.* (19, 20) showed CdA<sub>2</sub> adopts a pseudo-herringbone orthorhombic lattice (Fig. 2A) with longer ranged order at the higher pH. Lattice energy calculations show that the pseudo-herringbone packing is not as favorable as the herringbone packing; however, the difference in energy is less than that between the hexagonal packing and the equilibrium structure (5, 6). More important, as shown in Fig. 2B, the unit cell of the pseudo-herringbone packing is significantly smaller in the NN direction than the hexagonal or herringbone packing. In order for the high-pH pseudo-herringbone lattice to convert to the equilibrium structure, the lattice must expand in the NN direction to allow for rotation of the chain axes, which effectively takes the molecules through the hexagonal packing on the way to condensing into the equilibrium structure (Fig. 2A). This expansion likely requires an activation energy;

hence, the kinetics of the transition should be significantly slower, as is observed.

The consequences of this inhibited transition are shown in the molecular-resolution lattice images of the LB films shown in Fig. 4. An AFM image (Fig. 4A) of a five-layer film deposited at pH 7 shows that the as-deposited hexagonal structure has completely converted into the equilibrium herringbone structure. AFM and electron diffraction show that the typical grain size in CdA<sub>2</sub> films deposited at pH 7 is 10 to 100 μm (8, 12, 21). Figure 4B shows a five-layer film of CdA<sub>2</sub> deposited at pH 8.8. These films consist of many 5- to 10-nm-sized crystallites. Fourier transforms from various crystallites reveal lattice spacings corresponding to all three packings shown in Fig. 2A: (i) the equilibrium herringbone structure, (ii) the hexagonal packing, and (iii) the as-deposited pseudo-herringbone packing. The conversion between as-deposited and equilibrium lattice structure is inhibited by deposition from the high-pH subphase. Attenuated total reflection-Fourier transform infra-red (ATR-FTIR) spectra of five-layer CdA<sub>2</sub> films deposited onto germanium ATR crystals at high and low pH

**Fig. 3.** Overturning (top) and creeping (bottom) mechanisms of reorganization. After any two layers are deposited, the top bilayer consists of two opposed asymmetric monolayers (left). The black molecules represent CdL<sub>2</sub> and the gray molecules CdSt<sub>2</sub>. When the films overturn (top), the interior bilayer forms a headgroup-headgroup interface between two CdSt<sub>2</sub> monolayers. In the creeping mechanism, the alternate layering is preserved. The headgroup-headgroup asymmetric interface can transform to the centrosymmetric bilayer as in Fig. 2B. The expected step heights are significantly different for the two mechanisms and can be easily resolved by AFM (Table 1).

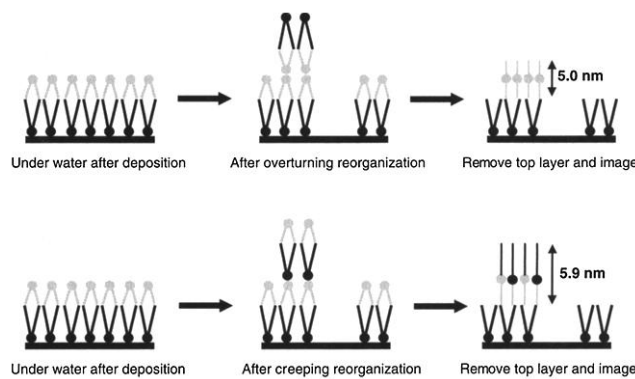


**Table 1.** Comparisons of predicted and actual island heights for two alternating layer films allowed to reorganize. In (1), a monolayer of CdSt<sub>2</sub> was deposited as described previously onto a silicon wafer at 25°C and a surface pressure of 30 mN/m, followed by a monolayer of CdL<sub>2</sub> deposited at 32°C and 30 mN/m. In (2) a monolayer of CdL<sub>2</sub> was deposited at 32°C and 30 mN/m, followed by a monolayer of CdSt<sub>2</sub> at 25°C and a surface pressure of 30 mN/m. Both (1) and (2) were allowed to reorganize at 25°C under water for 15 minutes. The resulting films were then removed through a clean air-water interface to strip off the top monolayer. This results in a film with monolayer and three-layer regions. All step heights measured were consistent with the overturning mechanism.

Film	Predicted		Measured
	Overturning	Creeping	
(1) CdSt <sub>2</sub> /L <sub>2</sub>	6.8	5.9	6.8 ± 0.4
(2) CdL <sub>2</sub> /St <sub>2</sub>	5.1	5.9	5.0 ± 0.3

**Fig. 4.** Molecular-resolution AFM images (14 nm by 14 nm) of five-layer CdA<sub>2</sub> films on silicon. (A) Film deposited at pH 7 shows only one crystal grain with measured lattice parameters,  $d_{02} = 0.375 \pm 0.004$  nm and  $d_{11} = 0.406 \pm 0.004$  nm, consistent with the herringbone structure (Fig. 2A). AFM and electron diffraction show that the typical grain size at pH 7 is of order 10 to 100 μm. (B) Film deposited at pH 8.8 shows numerous small crystallites. The nanocrystal labeled 1 has the herringbone packing, with measured  $d_{02} = 0.375$  nm and  $d_{11} = 0.406$  nm (12). The nanocrystal labeled 2 is hexagonal, with  $d$  spacings of 0.411, 0.416, and 0.412 nm, which compare well to the expected  $d_{02} = d_{11} = 0.41$  nm for the hexagonal phase (12). Nanocrystal 3 has the pseudo-herringbone packing with measured  $d_{02} = 0.391$  nm and  $d_{11} = 0.415$  nm; the expected  $d_{02} = 0.393$  nm and  $d_{11} = 0.415$  nm (5, 6). The error in the measured  $d$  spacings of these nanocrystals is about ± 0.01 nm due to the small size of the nanocrystals.

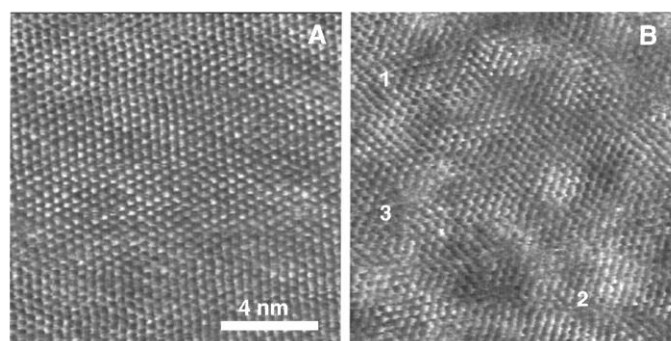


[figure available in supplementary material (22)] confirm this difference in the LB film structure. The inhibited transition also results in little to no decrease in the average area per molecule from the as-deposited to the final structure, so pinholes are minimized relative to the low-pH films (Fig. 1).

The reorganization is also likely inhibited by a dramatic increase in the monolayer viscosity at high pH as shown by canal viscometry. [Details of experiments are available; see (22, 23).] For the pH 7 monolayer, the monolayer viscosity was  $0.98 \pm 0.04$  dyne-s/cm, similar to that measured earlier for fatty acid films on cadmium subphases (24). However, at pH 8.8 the surface viscosity was  $41.8 \pm 0.93$  dyne-s/cm, a 40-fold increase, consistent with the increased ordering of the pseudo-herringbone structure (Fig. 2A). This higher viscosity of the monolayer requires a slower dipping speed for depositing the LB films.

Although the increased viscosity is likely due to the increased ordering of the alkane chains of the monolayer at pH >8.5, sum fre-

quency generation (SFG) spectroscopy (Fig. 5) shows that the water adjacent to the headgroup region is also better ordered. The SFG signal occurs only if there is a lack of inversion symmetry at the interface; any ordering of the water adjacent to the interface breaks the inversion symmetry and leads to the increased signal seen at the higher pH (25, 26). The more-ordered water layer could slow the rearrangement of the counterions necessary for the transformation from the as-deposited to the bulk soap structure, as well as contribute to the higher monolayer viscosity.

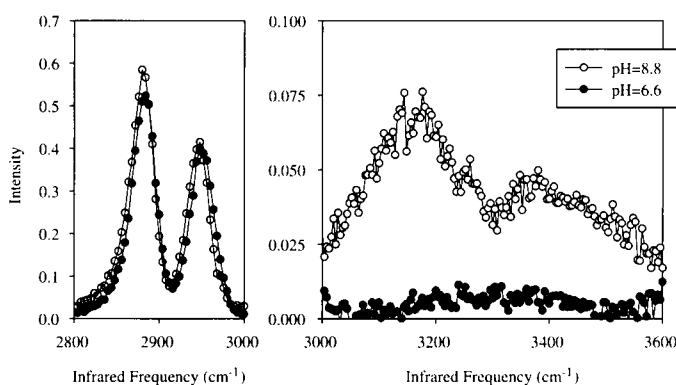
Figure 6A shows an AFM image of two monolayers of CdA<sub>2</sub> deposited at pH 7, transferred to a pH 8.8 subphase to soak for 1 hour, with a final monolayer deposited at the higher pH. In Fig. 6B, two monolayers were deposited at pH 8.8, allowed to soak for 1 hour at pH 7, with a final monolayer deposited at pH 7. The films initially deposited at pH 7 reorganized, whereas the films deposited at pH 8.8 did not, even when exposed to the lower pH. Reorganization is inhibited by

the lattice structure of the deposited film rather than the local conditions during the reorganization. Thus, it should be possible to prepare near-perfect LB films for specialized applications (such as sensors, waveguides, etc.) in nanotechnology using a two-stage deposition process.

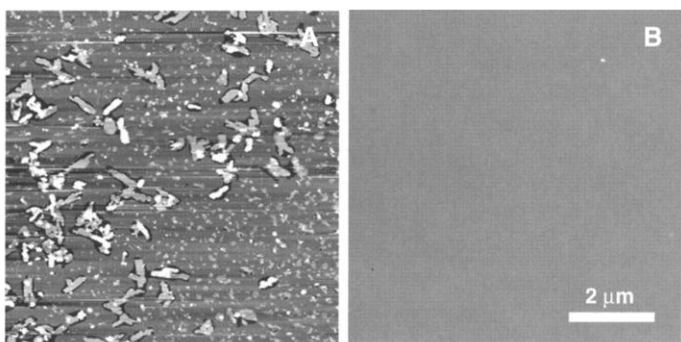
References and Notes

- G. G. Roberts, *Langmuir-Blodgett Films* (Plenum Press, New York, 1990).
- D. K. Schwartz, *Surf. Sci. Rep.* **27**, 241 (1997).
- G. J. Ashwell, *J. Mater. Chem.* **9**, 1991 (1999).
- T. L. Penner, H. R. Motschmann, N. J. Armstrong, M. C. Ezenyilimba, D. J. Williams, *Nature* **367**, 49 (1994).
- V. M. Kaganer, H. M $\ddot{o}$ hwald, P. Dutta, *Rev. Mod. Phys.* **71**, 779 (1999).
- I. Kuzmenko, V. M. Kaganer, L. Leiserowitz, *Langmuir* **14**, 3882 (1998).
- A. I. Kitaigorodskii, *Organic Chemical Crystallography* (Consultant Bureau, New York, 1961).
- J. A. Zasadzinski, R. Viswanathan, L. Madsen, J. Garnaes, D. K. Schwartz, *Science* **263**, 1726 (1994).
- XPS measurements were done by T. Mates using a Kratos Analytical XPS spectrometer (Chestnut Ridge, NY) on monolayers of cadmium arachidate deposited from subphases at either pH 7 or 8.8. The theoretical ratio of carbon to cadmium in CdAr<sub>2</sub> is 40:1; the measured ratios were 34:1 for the pH 7 films and 39:1 for the pH 8.8 films.
- D. K. Schwartz, R. Viswanathan, J. Garnaes, J. A. Zasadzinski, *J. Am. Chem. Soc.* **115**, 7374 (1993).
- P. Tippmann-Krayer, R. M. Kenn, H. Mohwald, *Thin Solid Films* **210/211**, 577 (1992).
- D. K. Schwartz, J. Garnaes, R. Viswanathan, S. Chiruvolu, J. A. Zasadzinski, *Phys. Rev. E* **47**, 452 (1993).
- D. K. Schwartz, J. Garnaes, R. Viswanathan, J. A. Zasadzinski, *Science* **257**, 508 (1992).
- R. W. Corkery, *Langmuir* **13**, 3591 (1997).
- D. K. Schwartz, R. Viswanathan, J. A. Zasadzinski, *J. Phys. Chem.* **96**, 10444 (1992).
- The hexagonal to pseudo-herringbone transition that occurs by increasing pH in CdAr<sub>2</sub> can also be induced by lowering the temperature to 7°C. For the longer chain cadmium behenate (C<sub>22</sub>), this transition occurs at about 20°C. In general, phase transitions of molecules with similar headgroups increase by 5° to 10°C for each additional two carbons in the chain. CdL<sub>2</sub> is in the low-viscosity, hexagonal phase at this deposition temperature, which is why it reorganizes.
- D. G. Wiesler *et al.*, *Thin Solid Films* **266**, 69 (1995).
- P. Ganguly, M. Sastry, S. Choudhury, D. V. Paranjape, *Langmuir* **13**, 6582 (1997).
- F. Leveiller *et al.*, *Science* **252**, 1532 (1991).
- F. Leveiller *et al.*, *Langmuir* **10**, 819 (1994).
- J. G. Garnaes, D. K. Schwartz, R. Viswanathan, J. A. Zasadzinski, *Nature* **357**, 54 (1992).
- Web figure 1 is available at Science Online at [www.sciencemag.org/cgi/content/full/293/5533/1292/DC1](http://www.sciencemag.org/cgi/content/full/293/5533/1292/DC1).
- W. D. Harkins, J. G. Kirkwood, *J. Chem. Phys.* **6**, 298 (1938).
- M. Yazdaniyan, H. Yu, G. Zografi, M. W. Kim, *Langmuir* **8**, 630 (1992).
- D. E. Gragson, G. L. Richmond, *J. Phys. Chem. B* **102**, 3847 (1998).
- P. B. Miranda, Q. Du, Y. R. Shen, *Chem. Phys. Lett.* **286**, 1 (1998).
- Y. R. Shen, *Annu. Rev. Phys. Chem.* **40**, 327 (1989).
- Preliminary viscosity measurements were done by J. Ding. Financial support for this project was provided by the National Institutes of Health (GM47334 and HL51177), the Tobacco Related Disease Research Program (8RT-0077), and the Materials Science and Engineering Research Center program of the NSF (DMR-9632716).

**Fig. 5.** SFG spectra of the CH (2750 to 3000 cm<sup>-1</sup>) and OH stretch region (3000 to 3800 cm<sup>-1</sup>) for monolayers of cadmium arachidate on 0.6 mM cadmium chloride subphases buffered at pH 6.6 (closed circles) and pH 8.8 (open circles). The theory and experimental setup of SFG have been described in detail elsewhere (25–27). The strong signal intensity at both pH values from the CH<sub>3</sub> symmetric stretch (at 2870 cm<sup>-1</sup>) and its Fermi resonance (at 2945 cm<sup>-1</sup>) without a CH<sub>2</sub> stretch indicate that the chains are in the all-trans configuration. The difference in absolute CH region intensities between low and high pH is the result of constructive interference between the water peak at 3200 cm<sup>-1</sup> and these peaks. The peak near 3200 cm<sup>-1</sup> in the high-pH spectrum is attributed to a high degree of hydrogen bond order (ice-like structure) of the water adjacent to the interface (25–27). The second, smaller peak near 3400 cm<sup>-1</sup> has been attributed to a more liquid-like arrangement of the water (25–27). The intensity of both the water-like and ice-like peaks fall to almost immeasurable values in the low pH case showing that the water layer is indeed much more poorly ordered. All data were taken with a 22-ps Nd:YAG (Nd-yttrium-aluminum-garnet) laser using the SSP polarization combination.



**Fig. 6.** AFM images (12 μm by 12 μm) of CdA<sub>2</sub> deposited and equilibrated in different pH subphases. (A) First, two layers were deposited at pH 7, then the film was transferred to a pH 8.8 subphase. The film reorganized, which is what we expect for films deposited from the hexagonal structure present at the air-water interface at pH 7. (B) First, two layers were deposited at pH 8.8, then the film was transferred to a pH 7 subphase. The film did not reorganize, which is what we expect at high pH.



20 February 2001; accepted 3 July 2001